ACS OMEGA

Open Access

http://pubs.acs.org/journal/acsodf

Article

Synthesis of Graphene Nanosheets from Coconut and Candlenut Shells: Large-Scale Production and Application in Fe Ion Adsorption and Electrochemical Properties

Yosia Gopas Oetama Manik, Boon Tong Goh, Rikson Siburian,* and Yatimah Alias

Cite This: *ACS Omega* 2025, 10, 3338−3350

Read Online

ACCESS | Metrics & More | Article Recommendations | Supporting Information

ABSTRACT: Graphene nanosheets (GNS) have garnered significant attention due to their exceptional properties and wide-ranging applications. This research aims to synthesize GNS from coconut shells and candlenut shells and to compare their performance in Fe ion adsorption and electrochemical properties. Both coconut and candlenut shells were used as raw materials, and the pyrolysis method was chosen to produce large-scale GNS. The GNS were characterized using Raman spectroscopy, X-ray diffraction, FTIR, FESEM-EDX, AAS, and electrochemical measurements, including CV and EIS on modified electrodes. New findings from this study reveal that GNS derived from candlenut shells exhibit thinner layers and fewer defects compared with those derived from coconut shells. This structural advantage contributes to superior Fe ion adsorption efficiency and better electrochemical performance, making the GNS from candlenut shells more suitable for applications in flexible electronics and electrochemical devices. Furthermore, the synthesis method effectively reduces the amount of oxides associated with defects in the GNS, enhancing the material's potential for high-performance applications. The GNS produced from candlenut shells showed an Fe adsorption effectiveness of 0.33 ± 0.012 mg/g, a charge transfer resistance of 0.78 kΩ, and a capacitance of 108.8 F/g, indicating their promising role in future technological applications.

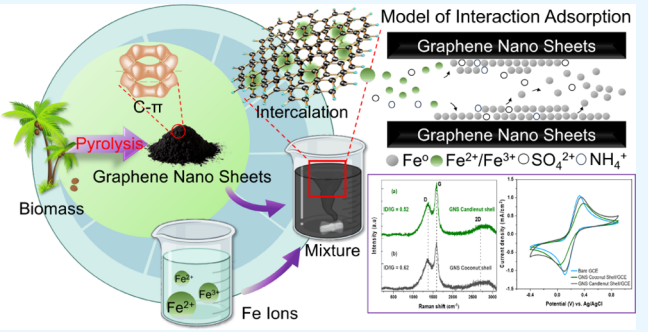

INTRODUCTION

Carbon nanoallotropes produce cutting-edge and multi-application carbon materials such as carbon dots, graphene, carbon nanotubes (CNTs), fullerenes, carbon nanoforms, nanocapsules, carbon nanofibers, and carbon nanobuds. Graphene is the thinnest 2D material with a thickness of one carbon atom, and it possesses outstanding properties: high electrical conductivity (1250 S/cm^2), large surface area (2600 m^2/g), and C-sp^2. Graphene, as a material with unique electrical properties, exhibits a lower sheet resistance than many other carbon allotropes, typically around 96 Ω/sq, which enhances its potential in various electronic applications.[1] Graphene has a distinctive electronic structure where the valence and conduction bands intersect at the Dirac points within the hexagonal Brillouin zone, particularly at the K point. This intersection results in graphene being a gapless material, posing challenges for its direct use as a semiconductor. However, this unique electronic structure also facilitates the high mobility of electrons and metal ions within the graphene lattice. Therefore, it is necessary to modify graphene by doping heteroatoms of metallic elements such as Ni, Fe, Mg, and Cu,[2−5] and nonmetals like B, N, P, and S to overcome the zero band gap.[6] Graphene possesses a notably elevated theoretical specific surface area, enabling the incorporation of additional active sites to facilitate electrochemical reactions. In the literature, the specific capacitance of graphene often falls significantly short of its theoretical value of 550 F g^{-1}. This discrepancy can generally be attributed to two main factors. First, during the implementation of supercapacitors, restacking of graphene layers occurs due to $\pi-\pi$ interactions, diminishing the specific surface area and impeding ion diffusion within the active material.[7] Second, the conductivity of graphene is hindered by structural defects such as imperfect graphene and the introduction of heteroatom-containing groups during synthesis.[8] Consequently, these factors diminish the power density and rate performance of graphene-based supercapacitors. Additionally, graphene has been applied as an electrochemiluminescence (ECL) sensor.[9] Transistors, water filtration, solar cells, drug delivery systems, biosensors, and biomedicine notably impact the immune system,[10−12]

Received: June 19, 2024
Revised: November 29, 2024
Accepted: December 12, 2024
Published: January 17, 2025

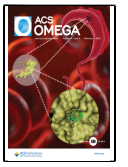

The top-down approach from commercial graphite mostly synthesizes graphene through various techniques, namely, mechanical and chemical exfoliation methods. Previous research has shown that graphene can be synthesized in addition to graphite, namely, from coal and petroleum (nonrenewable resources). On the other hand, graphene can also be synthesized from coconut shells,[13] coffee grounds,[14] and rice husk,[15] and other biomass (renewable resources) are also sources of carbon in graphene synthesis. Many manufacturing methods for graphene have been proposed for waste sources, especially plant and biomass,[16] one of which is the chemical vapor deposition (CVD) method; a single layer of graphene is produced, where the thickness of graphene produced, namely, one carbon atom, has good quality and good properties.[5] However, this method has the disadvantage of a small number of products due to the limited area of metal substrate catalysts and the size of CVD reactors.[17] Reduced graphene oxide (RGO) is widely developed using the Hummer modification method, where commercial graphite is oxidized into graphene oxide using the oxidizing agents H_2SO_4, $NaNO_3$, $KMnO_4$, and H_2O_2 and reduced again by a reducing agent and then rinsed with water to obtain a reduced graphene oxide-produced graphene multilayer. The modified Hummers method involves graphene synthesis by oxidizing graphite to break interlayer bonds, causing the formation of oxygen functional groups, epoxy, hydroxy, and carboxyl groups due to the release of positive metal ions from strong oxidizers, followed by the removal of acidic compounds and the production of graphene oxide. The large number of oxide, epoxy, and carboxyl groups bound to graphene oxide results in a low C/O ratio, low electrical conductivity, and low mechanical properties due to structural distortion. The reduction of graphene oxide (GO) is crucial for restoring graphene's intrinsic properties, including its high electron mobility.[18,19] We have previously employed the modified Hummer method to synthesize GNS from graphite; however, this approach has several limitations, including low production yield (approximately 30−40% mass ratio), long processing times (around 1 week per cycle), and the extensive use of hazardous chemicals.[20] Moreover, exfoliation methods have developed for 2D materials such as electrochemical exfoliation, mechanical exfoliation, liquid phase, or involving complex methods to produce graphene; furthermore, each method has distinct advantages and limitations, influencing the structural properties; however, the material used is graphite, which will be peeled off to produce a layer of graphene.

Graphene synthesis from biomass using the pyrolysis method was carried out. Interestingly, the mechanism underlying the synthesis process has not been fully elucidated, and the deflagration phenomenon is interesting because the pyrolysis process involves a transition in the form of hybridization of C-sp^3 carbon to C-sp^2, and an increase in the percentage of graphitic carbon influenced by increasing temperature.[21] This method has been widely studied using biomass and other waste carbon sources because the pyrolysis method is eco-friendly and has diverse applications. The pyrolysis method successfully synthesized large-scale N-GNS and GNS from coconut shells. The results validated by TEM showed a flat surface with an N-graphene lattice distance of 0.36 nm and a graphene lattice distance of 0.34 nm. This method is considered less expensive and more environmentally friendly and could be applied on a large-scale production.[22] In a comparison of the graphene production method from pyrolysis with other studies, this research stands out for using biomass waste as the primary feedstock without involving hazardous chemicals like strong oxidants, making it more environmentally friendly and suitable for sustainable approaches. However, challenges remain in optimizing the quality and controlling the structural integrity of the resulting graphene. On the other hand, the intermediate-assisted grinding exfoliation (iMAGE) method demonstrates advantages in exfoliation efficiency, producing large lateral-sized, high-quality graphene, but it requires specialized equipment and intermediary particles (such as SiC), adding complexity and production costs.[23] Additionally, the review by Munuera et al. emphasizes the importance of using life cycle assessment (LCA) to evaluate the environmental impact of various graphene production methods, including pyrolysis and liquid-phase exfoliation, with a focus on using waste materials as carbon sources.[16] While this approach holds promise for sustainability, certain methods, such as CVD, still face challenges related to high energy consumption and scalability issues. Overall, the method used in this study offers a more eco-friendly and cost-effective solution, but further improvements are needed to ensure consistent quality for broader commercial applications.

Functionalized groups in graphene such as oxygen-containing groups significantly impact the conductivity of graphene. The introduction of oxygen functional groups leads to a reduction in thermal conductivity due to enhanced phonon scattering, limiting the phonon mean free path and increasing phonon-defect scattering.[24,25] Additionally, exposure to oxygen can cause local oxidation of graphene, decreasing its roughness, conductivity, mechanical resistance, and frictional characteristics, ultimately affecting device performance.[26,27] Hence, reducing agents play a crucial role in the synthesis of graphene. Different reducing agents used in the reduction of graphene oxide (GO) lead to variations in the carbon-to-oxygen ratio, carbon lattice defects, and the distribution of oxygen groups. Additionally, the reduction process affects the stacking nanostructure, interlayer distance, and content of oxygen groups, ultimately influencing its properties such as specific capacitance and energy density in supercapacitors. Various reducing agents like alkali rare earth metals, thermal treatment, tetraethylenepentamine (TEPA), hydrazine hydrate, hydroiodic acid, hydrazine, glucose, urea, and sulfur acid-derived, are commonly used.[24,28,29] In this study, a novel reducing agent, namely, activated charcoal (AC), was used. According to the results of research on activated commercial charcoal containing chromium, cadmium, aluminum, and small amounts of metals such as Pb, Zn, and Mn.[30] Metals can react with oxide groups to form metal oxides, making it possible to reduce the number of oxide groups on the surface of carbon materials with metal−oxide interactions, which is expected to reduce the amount of oxygen. For instance, the use of AC as a reducing agent will provide a simple and environmentally friendly approach for reduction graphene synthesis. Overall, the choice of reducing agent significantly influences the efficiency, cost-effectiveness, and environmental impact of the graphene synthesis process. Commonly, graphene synthesis from graphite by each method has defects that may give unique properties; however, lignocellulosic content in biomass has a potential for graphene material.[31,32]

In materials, the candlenut shell is a waste from the candlenut industry. Generally, candlenut seeds are used as kitchen spices, candlenut oil, and traditional medicine; the

https://doi.org/10.1021/acsomega.4c05745
ACS Omega 2025, 10, 3338−3350

discarded shells have a hard and dense texture. Research has focused on utilizing carbonaceous agricultural waste, such as candlenut shells, which are abundant in Indonesia. It has been reported that Indonesia's annual production of candlenuts has reached 100,700 t. In addition to Indonesia, according to FAO statistics, global candlenut production in 2020 amounted to 554,490 t. Given that approximately 66.1% of candlenut comprises shells, considered solid biowaste, an estimated 366,518 t of waste are generated from candlenut production annually.[33] Agricultural waste is a cost-effective and environmentally sustainable alternative source of carbon for the production of nanoscale electronic devices.[34] Utilizing candlenut shells to produce GNS offers dual benefits: it reduces agricultural waste and lowers the cost of GNS production. The properties of GNS derived from agricultural waste depend on the preparation method. Biowaste-derived graphene shows promise as an adsorbent for removing heavy metals from aquatic environments due to its large surface area. Recent studies of graphene synthesis through pyrolysis of candlenut shells show promising results, where the resulting GNS is close to commercial graphene;[35] thus, the development under pyrolysis environmental conditions can control the resulting graphene's properties.[36] In this work, we conducted the pyrolysis process at a vacuum level below 1 mbar to see any changes in the crystal structure and performance of the produced graphene.

Iron (Fe), a heavy metal found in soil, can dissolve in rainwater, increasing the metal concentration in water. Interestingly, graphene is more efficient in water filtration.[37] The adsorption of Fe ions on graphene is driven by a complex interplay of various physicochemical processes including electrostatic interactions, ion−π interactions, and surface complexation reactions. The mechanism of Fe ion adsorption on graphene can be broadly divided into several stages: (1) the initial transport of Fe ions from the bulk solution to the graphene surface, (2) the adsorption of Fe ions on the graphene surface through various binding mechanisms, and the potential formation of secondary precipitates or complexes. Previous studies on Fe-doped graphene generally utilize graphite as the primary material.[3,38,39] In contrast, our research explores the synthesis of graphene from biomass sources, which could lead to unique structural characteristics and enhanced properties in adsorption and electrochemical applications due to the specific defect structures inherent in biomass-derived graphene. Therefore, it is important to explore the synthesis, characteristics and development of our prepared GNS. In this paper, GNS were synthesized from candlenut and coconut shells; we also elaborate on the mechanism of our synthesis method and the relationship between adsorption ability and electrochemical properties

RESULTS AND DISCUSSION

Mechanistic Synthesis of GNS. GNS was synthesized from biomass waste. According to previous research, coconut shell biomass has abundant carbon sources, such as hemicellulose (31.80%), lignin (44.7%), and cellulose (15.13%).[40] Conversely, the candlenut shell has lignin (54.6%) and cellulose (49.2%),[41] which significantly affects the structure, electrical, and electrochemical properties of the graphene-synthesized. These feedstocks demonstrate significant potential as carbon precursors for graphene synthesis. Previous studies have utilized coconut shell waste through thermal and pyrolysis methods to produce graphene.[22,42] We emphasize the use of candlenut (*Aleurites moluccanus*) as the biomass precursor for the synthesis; candlenut produced the highest yield of 21% (w/w) (from fresh biomass), as shown in Table S1. This is comparable to other methods, such as the electrochemical method yielding 20 wt %,[43] chemical exfoliation achieving 100%,[44] and ball milling with supercritical fluids yielding 90%.[45] However, our method, which uses biomass without the need for strong acid or base treatments, stands out as the eco-friendly, cheap, and scalable approach, promising for large-scale production. Biomass generally exhibits an amorphous structure (Figure 8B). This approach involves the pyrolysis of coconut shell charcoal, leading to the formation of carbon materials, including graphite oxide. Subsequent reduction processes are required to convert these oxides into graphene nanosheets (GNS), making it a more environmentally friendly (green) synthesis route. The main way to obtain GNS is through pyrolysis and the reduction of oxide groups with AC. First, the cracking process involves using aluminum foil as a catalyst under low-temperature heating, facilitating electron transfer from aluminum, which acts as a Lewis base.[46] This electron transfer promotes the reduction of carbon materials, an irregular accumulation of electrons, and then cracking.[42] During pyrolysis, the biomass undergoes thermal decomposition in an Ar atmosphere; the shells were slowly pyrolyzed at a temperature of 600 °C with a heating rate of 5 °C/min. In this process, carbon compounds decompose into simpler forms due to the breaking of organic bonds. As the temperature surpasses 200 °C, water content evaporates, and further heating breaks the oxygen bonds in cellulose and lignin, releasing aldehydes, carboxylates, hydrogen, and volatile gases as byproducts.[47,48] Carbon decomposition and restructuring occur, resulting in crystal phase changes, as shown in the XRD data (Figure 8C). Several sharp and narrow peaks were observed at 2θ = 27°, which closely aligns with the characteristic peak of graphite at 2θ = 26°, indicating an interlayer spacing of approximately 0.334 nm.[49]

Under the effect of AC, the second stage of pyrolysis was conducted at the same temperature for a shorter time to determine the effect of AC as a reducing agent. Energy is provided so that the reaction occurs, where activated carbon is used as a reducing agent. Interestingly, the active metal group on carbon may bind to the oxide on graphite oxide, mostly through inorganic chemical compounds that can reduce oxide groups, such as Zn, Al, Fe, and Mg. The AC contained metals such as Zn, Cr, and Cd.[30] These various metals can reduce oxygen functional groups; oxide must be reduced in order to restore the π network, and the electrons of metals bind to free electron oxygen functional groups. During pyrolysis, the presence of impurities or functional groups such as oxygen, which bind to metals as ligands,[50] promotes the transition of carbon atoms from sp^3 to sp^2 hybridization. This transition alters various properties of the resulting carbon structure, including interlayer spacing, defect density, elemental composition, and the C/O ratio. The shift toward sp^2 hybridization is driven by the elimination of oxygen groups and structural reorganization. Additionally, reducing agents can further influence these parameters, affecting the material's structure and electrical properties. Further characterizations, including Raman spectroscopy, XRD, FTIR, FESEM, and TEM, were conducted to investigate these properties.

Raman Study. Raman spectroscopy is a powerful and reliable characterization technique that provides nondestructive and rapid information about the structure of nanomateri-

https://doi.org/10.1021/acsomega.4c05745
ACS Omega 2025, 10, 3338−3350

als. It is commonly used to study defects, crystallite size, and the number of layers of sp^2 hybridized carbon and its allotropes. In the case of GNS, Raman spectroscopy is particularly useful to analyze their structural properties and confirm the quality of the synthesized material. GNS has three major peaks, namely the D band at ~1350 cm^{-1}, the G band at ~1580 cm^{-1}, and the 2D band at ~2790 cm^{-1}.[13,51] Based on Figure 1, GNS has the same point bands indicated structure

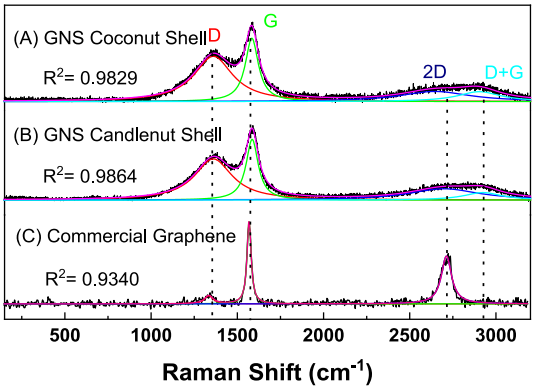

Figure 1. Raman spectra of GNS coconut (A); candlenut (B); and commercial graphene (C).

GNS approach to graphene structure;[52] however, the 2D band shows a broader band that indicates stacking graphene layers on GNS much more thicker (multilayer). The displayed Raman scattering spectra were measured within the range of 200−3200 cm^{-1}. Specifically, the line corresponding to the 2D band fell within the 2600−2900 cm^{-1} range. The average domain size of sp^2 carbon in GNS was calculated by relating the ratio of the intensities of the D and G bands using the Tuinstra and Koenig relation eq 1:[53]

$$\frac{I_D}{I_G} = \frac{2x10^{-10}(\lambda^4)}{L} \quad (1)$$

where L is sp^2 domain size, λ is the laser wavelength, which was used for Raman spectroscopy measurement, and I_D/I_G is the intensity ratio of the D and G peaks

Siburian et al. have synthesized GNS from coconut shells via pyrolysis showing Raman analysis on GNS has low-intensity 2D and ratio I_D/I_G.[22] due to defects on graphene giving change in weight, intensity, and even shift of peak. A defect on the lattice makes the weight broader; according to Figure 1, commercial graphene is narrower than GNS. GNS has defects on the lattice or edges due to unclear pyrolysis; the feedstock contains other functional groups such as hydroxyl, acetyl, carbonyl, aliphatic hydrocarbon, aromatic functional, and few metal traces such as Ca and K shown in Figures 3 and 4B, 5B. To measure the defects among the materials, we have calculated the full width at half-maximum (fwhm) number via Lorentzian fitting, as tabulated in Table 1.

The investigation of fwhm is essential for comprehending the structure properties of graphene, as it offers valuable insights into several elements of this material. fwhm analysis can be employed to assess the electrical properties of graphene, including its surface conductivity.[54] As seen in Table 1, GNS coconut has a D fwhm of 271.8825 cm^{-1} and the GNS candlenut peak has an fwhm number lower than coconut. This number depends on the peak width. This is influenced by interlayer coupling, edge roughness, strain, unintentional doping, and lattice imperfection.[55,56] We calculate the fwhm number against each bands. In graphene, the existence of defects in the crystal lattice of the materials led to the attribution of the D band, indicating a broken symmetry in the hexagonal carbon structure.[57] The G band signifies the presence of well-organized graphitic carbons, and the 2D band is utilized to distinguish the number of layers of the carbon structure.[58] The ratio of the G and 2D band intensities and the full width at half-maximum of the 2D band can determine the number of graphene layers.[59] The research conducted by Nor et al. uses the ratio I_{2D}/I_G and the peak's fwhm values to estimate the number of layers in graphene, ratio I_{2D}/I_G greater than 1 suggests a single-layer of graphene sheet or flake for variation I_{2D}/I_G exhibits a range of fluctuation from 1.12 to 0.89, indicating the distribution of graphene nanoplatelets with a thickness of 2−6 layers.[60,61] The commercial graphene I_{2D}/I_G ratio of close to 0.89 indicates that the reference graphene is few-layer graphene (FLG). However, GNS has an I_{2D}/I_G ratio of 0.31 for candlenut and 0.28 for coconut, respectively, indicating these graphenes are multilayer graphene (MLG) due to the decreasing ratio of I_{2D}/I_G results in an increase in the number of graphene layers.[62] This ratio confirms that number GNS candlenut's ratio is higher, which means relatively fewer layers more than coconut. Interestingly, these GNSs possess a D+G band that is absent in the reference material due to faults in the carbon material's graphitic structure.[63,64] The ratio of I_D/I_G is a crucial indicator of the degree of graphitization in carbon materials; it signifies a higher level of disorder or defects in the carbon structure, indicating a lower level of graphitization. Conversely, a lower I_D/I_G ratio corresponds to a more ordered carbon structure, reflecting higher graphitization levels.[63] Based on the ratio I_D/I_G shown in Table 1, the GNS candlenut shell is lower than the reference but better than the GNS coconut, which suggests a high degree of graphitization and a lower number of defects. However, these defects not only offer a way to tune the properties of graphene but also provide opportunities for novel functionalities and applications, showcasing the versatility and potential of defect engineering in graphene materials. XRD studies were carried out to corroborate the evidence for studying the crystal structure.

XRD Study. XRD analysis was carried out to compare the phases of the GNS crystals synthesized from coconut shell to those synthesized from candlenut shell under the same conditions at 600 °C. The observed broad and weak peak results suggested the existence of a nanoscale graphene layer

Table 1. Summary of Raman Spectra Analysis of GNS and Commercial Graphene

Sample	I_D/I_G	I_{2D}/I_G	D fwhm (cm^{-1})	G fwhm (cm^{-1})	2D fwhm (cm^{-1})	D+G fwhm (cm^{-1})
GNS Coconut Shell	0.6420	0.2820	271.8825 ± 2.5945	92.2714 ± 0.8826	493.7768 ± 21.7446	301.396 ± 18.2148
GNS Candlenut Shell	0.6167	0.3146	265.8653 ± 2.2070	85.4781 ± 0.6919	496.3931 ± 16.0278	265.8443 ± 20.3329
Commercial Graphene	0.1093	0.7261	60.6135 ± 12.222	28.9287 ± 0.8080	71.8613 ± 2.1197	-

https://doi.org/10.1021/acsomega.4c05745
ACS Omega 2025, 10, 3338−3350

on the interlayer,[65] both of which have the same C(002) peak. The diffraction peaks should satisfy the Bragg equation eq 2[35]

$$2d\sin\theta = n\lambda \quad (2)$$

The lattice spacing, represented by d, the angle θ formed between the inverse ray and the reflective crystal plane, the wavelength denoted by λ, and the reflection series numbered n all play crucial roles. The decreased spacing of the graphene layers can be attributed to increased disorder and damage within the crystal structure during the graphene preparation process. This suggests that graphene comprises multiple layers.

As seen in Figure 2, the GNS, coconut shell, and candlenut shell patterns, peaks at 2θ Bragg angles, C (002) diffraction

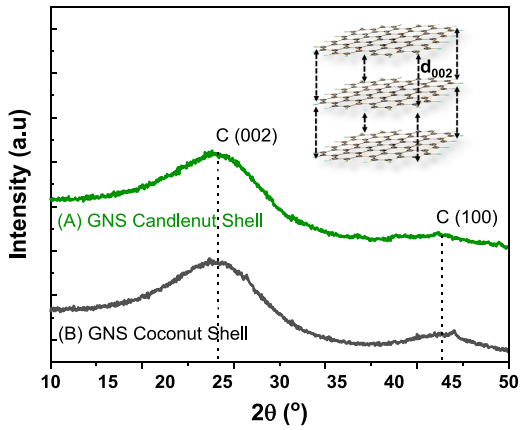

Figure 2. XRD diffractograms of GNS candlenut (A) and coconut (B).

peak at 2θ = 24.9°, interlayer spacing = 0.357 nm, and C (100) peak at 2θ = 44.24°, interlayer spacing = 0.409 nm confirmed the formation of GNS,[65−68] which is close to that of graphite at 2θ = 26° due to an interlayer spacing of 0.334 nm, JCPDS card no. 00−052−1907. Shifting can happen for several reasons, including exfoliation, graphite structural flaws, heating, the presence of vacancies and interstitials, and intercalation with other materials. The displacement of the (002) peak in the diffraction pattern of graphene is affected by both the degree of graphite oxidation and the thermal treatment.[69] Interestingly, GNS candlenut shells show lower intensity at C (100) than GNS coconut shells, assuming a more intense peak at C(100) due to decreased oxygen functional groups[65] Furthermore, as the layer number decreases,[66] each biomass has a different chemical quantity, and the candlenut shell is a feedstock with high lignin content. This carbon is harder to decompose than cellulose.[70] These compounds were confirmed using FTIR, as shown in Figure 3, so they also have different optimal conditions for transforming organic compounds into GNS structures.

FTIR Study. The functional groups were verified using FTIR spectroscopy. The IR radiation in FTIR can influence the impact of atomic vibrations on the specific adsorption and transmission of energy, which is helpful in determining particular molecular vibrations in a sample. The FTIR range we used was 4000−600 cm^{-1}. This study provides information on the elimination of oxygen-containing functional groups after and before the reaction and validates GNS functional groups. Biomass has various functional groups such as −OH, −NH, −CN, and so on. The presence of N-containing compounds within proteins was detected by the presence of peaks at 3600−3000 cm^{-1} and 1600−1500 cm^{-1} in the spectrum.[47] As seen in Figure 3, coconut and candlenuts have lignocellulose

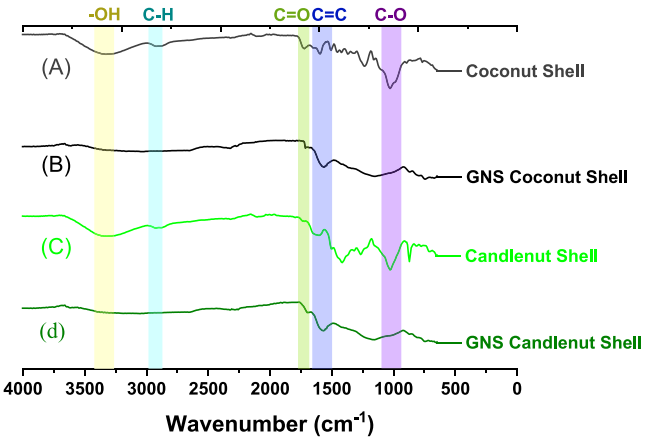

Figure 3. FTIR spectra of GNS coconut (A); coconut shell (B); GNS candlenut (C); and candlenut shell (D).

compound, which indicates from some of the spectra such as at ∼3317 cm^{-1} presence of O−H stretching of water, ∼2899 cm^{-1} presence C−H vibrations of aliphatic, ∼1714 cm^{-1} presence C═O stretching vibration of lignocellulosic carbonyl groups, ∼1604 cm^{-1} presence C═C stretching vibration. Interestingly, seen from the absorption of 1500−1600 cm^{-1}, the lignocellulose region shows significant differences between coconut and candlenut, where the tendency of candlenut has many lignin compounds so that the absorption intensity of 1500 cm^{-1} is sharper than 1600 cm^{-1}, lignin has aromatic C═C compounds that bind to other organic compounds. After treatment, the functional groups significantly changed, and the functional groups became flat peaks, which means the success of the functional groups decreased. The product peaks at 1587 cm^{-1}, indicating that C═C aromatics successfully exist in the GNS coconut and candlenut shells.[13,71] The C sp^2 aromatic peak at 1587 cm^{-1} is clear, and interestingly, the sharp C═O and C−O peaks become weaker and disappear, confirming that the method can release the oxygen functional groups contained in the sample.

FTIR may be used to elucidate mechanisms based on functional groups lost or changed before and after treatment. First, coconut and candlenut shells have a broad band at 3364 cm^{-1}. This band confirmed the presence of hydrate (H_2O), hydroxyl (−OH), or amino groups following the presence of peaks at 1500−1000 cm^{-1}. After the first stage of pyrolysis, thermal treatment can eliminate water, CO, CO_2, alcohol, phenol, and CH_4. Second, pyrolysis in small quantities still produces gaseous products CO_2, light C^{2+} aliphatic hydrocarbons, and light aromatics. In this step, we added AC to prevent excessive release of carbon gas and succeeded as a catalyst for removing bound oxides, as evidenced by the XRD results in Figure 2. The strong C sp^2 aromatic peak and weaker carbonyl functional groups indicate that impurities, such as oxygen groups, are released, resulting in an electron-rich GNS.

Morphology and Elemental Studies. GNS coconut and candlenut shells were characterized by using FESEM-EDX to observe the morphology of the surface and to determine the elemental distributions, such as carbon, oxygen, and other elements, via EDX. GNS are conductive materials that can be easily characterized via FESEM to study their morphology and

https://doi.org/10.1021/acsomega.4c05745
ACS Omega 2025, 10, 3338−3350

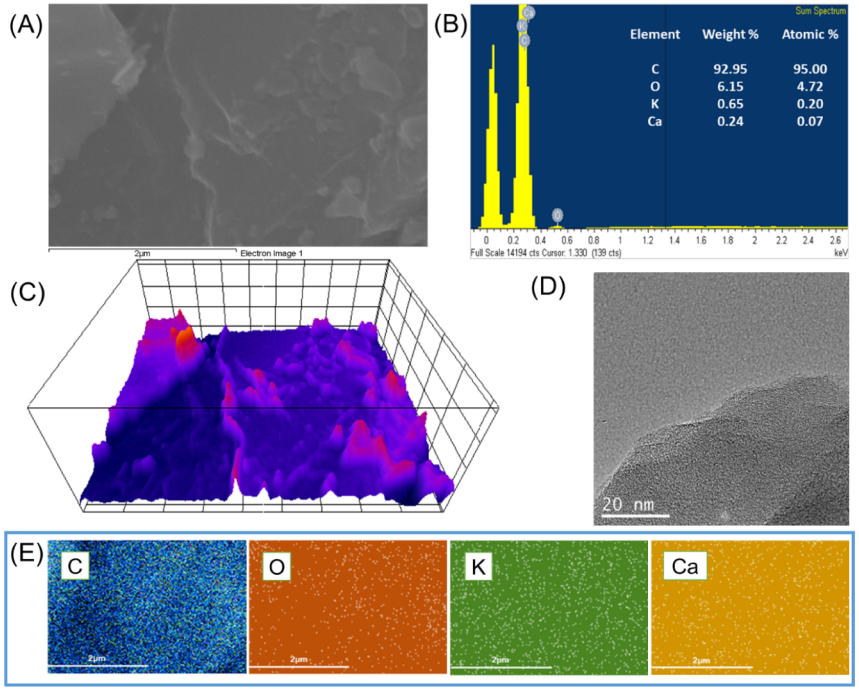

Figure 4. SEM image of GNS candlenut (A); EDX GNS candlenut (B); 3D Image of SEM GNS candlenut (C); and TEM Image of GNS candlenut (D) and mapping GNS candlenut (E).

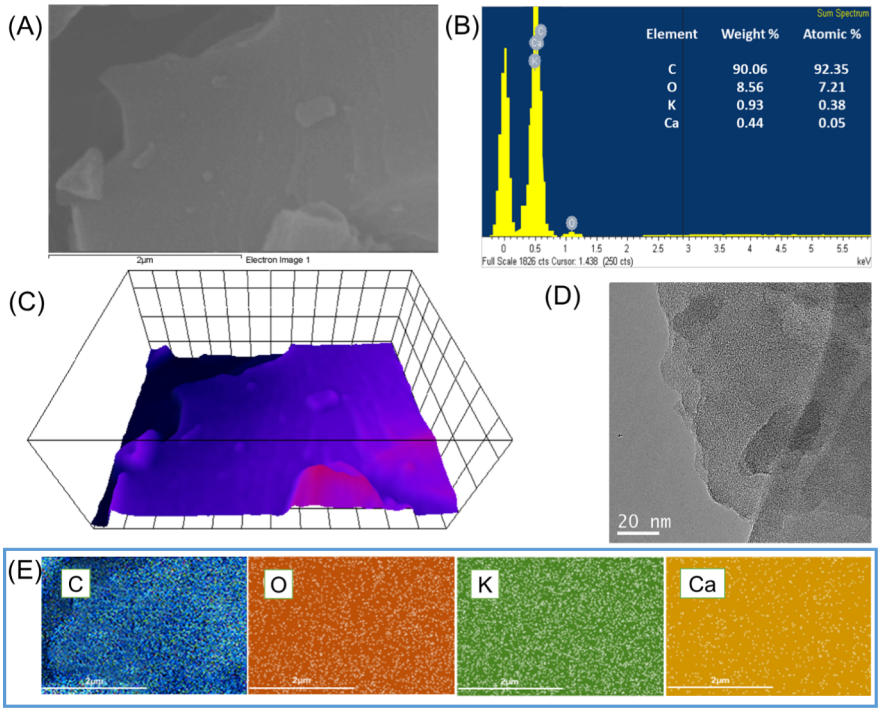

Figure 5. SEM image of GNS coconut (A); EDX GNS coconut (B); 3D Image of SEM GNS coconut (C); TEM Image of GNS coconut (D) and mapping GNS coconut (E).

structural characteristics. FESEM was integrated with EDX to analyze the chemical composition of the material. Energy-dispersive X-ray spectroscopy (EDX) was used to identify the elements present in the sample and determine the distribution of the elements within the material; both our GNS contained carbon, oxygen, potassium, and calcium, shown in Figure 4B for candlenut and Figure 5B for coconut.

The percentages of C (92.95%), O (6.95%), K (0.65%), and Ca (0.24%) in the GNS candlenut shell are shown in Figure 4B, and according to GNS coconut, we confirm the percentage of C (90.06%), O (8.56%), K (0.93), and Ca (0.05%) is shown in Figure 5B. Based on the EDX results, our product contains a high amount of C, which is appropriate for use with GNS composed of carbon; moreover, the sample contains other impurities, such as K and Ca alkaline earth metals, due to the

https://doi.org/10.1021/acsomega.4c05745
ACS Omega 2025, 10, 3338−3350

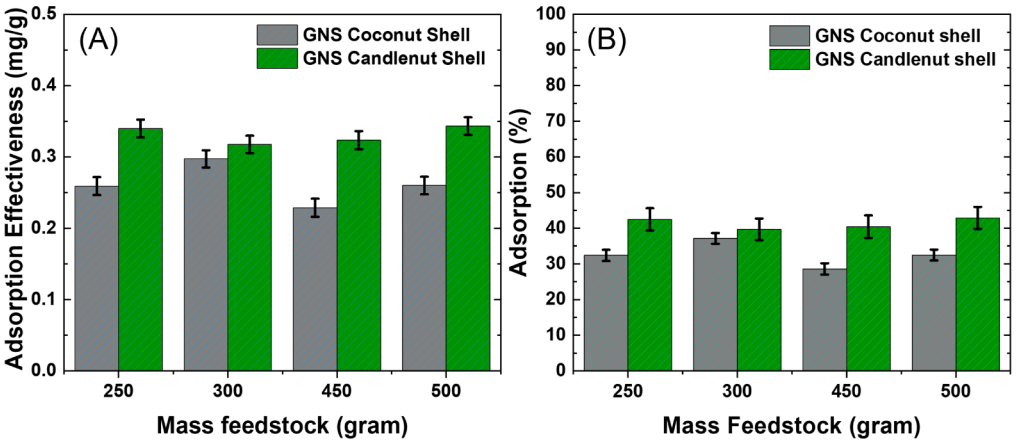

Figure 6. Diagram of the percentage of adsorbed Fe metal on GNS (A) and the effect of adsorption on GNS (B).

feedstock contains impurities. According to Kabir et al. research, coconut shells contain abundant metals such as potassium (42.5%) and calcium (17.4%).[72] Compared to the EDX of GNS coconut shown in Figure 5B, our result successfully decreases the trace metals. Interestingly, our method massively reduces impurities, and we assume that AC binds other elements, such as C-sp^3, which interact with metal groups and are solved by a solvent to separate any impurities attached to the surface of graphene. Focused on the determination of the contained C element, candlenut, much more than coconut, may influenced by the compound content of raw material. This happens due to different degradation temperatures of lignin, cellulose, and hemicellulose, which may affect morphology and structure, as similarly conducted by Chen et al.'s research. The temperature ranges for the thermal degradation of cellulose, hemicelluloses, and lignin were 269−394 °C, 170−776 °C, and 127−791 °C, respectively.[73] It means that GNS may be obtained from the degradation of hemicellulose and lignin. Interestingly, candlenut has higher lignin than coconut. This degradation compound may influence the characteristic structural and morphology of GNS candlenut shown in Figure 4D lignin that undergoes decomposition, polymerization, aromatization, carbonization, and graphitization during the treatment process,[31] which is more organized and less stacking than GNS coconut.

Both GNS coconut and candlenut have slightly similar morphologies, which contain C, O, K, and Ca that are evenly distributed on the surface, validated by mapping images shown in Figures 4E and 5E, respectively. Transmission Electron Microscopy (TEM) is an essential characterization technique for analyzing graphene structure, providing insights into its structural, mechanical, and electronic properties at the atomic level.[74] Figure 4D displays TEM images of GNS from candlenut biomass, revealing a smooth, continuous sheet structure with few defects, indicating good crystallinity. In contrast, Figure 5D shows GNS from coconut biomass, which also exhibits a layered structure but with more irregular edges and thickness variations, suggesting a more heterogeneous material, which may indicate variations in the properties of the biomass or the extent of graphitization. TEM image reveals areas with higher contrast in some regions, indicating variations in thickness. Some layered structures can also be observed, suggesting that the graphene in this sample is more likely composed of multiple layers (multilayer graphene). The variation in contrast and texture suggests a more heterogeneous thickness distribution compared to that of GNS candlenut. The consistency in thickness across the samples, particularly at nanoscale dimensions (as indicated by the 20 nm scale bar), reinforces that the material falls within the graphene nanosheet range. Previous studies using High-Resolution TEM analysis have shown that graphene nanosheets have a transparent, holey structure with an interlayer spacing of about 0.34 nm.[74,75] This aligns with our findings, which also show that the GNS has a flat, thin-layered structure. This morphology is consistent with the crystal structure indicated by Raman and XRD data. Stacked graphene layers can exhibit different electrical and optical properties based on how they are arranged and other external factors affecting them.[64,76]

Fe Adsorption Study. Adsorption is the phenomenon in which ions from a substance stick to the surface of the material, conducted to Siburian et al.'s research loading Pt metal to GNS success deposit due to the interaction of chemicals on GNS. This research proves GNS can change metal ions to pure metal[20] to confirm properties of GNS. We calculated Fe metal using AAS.

From Figure 6, GNS is able to adsorb Fe metal. The percent average adsorption of GNS for coconut shells was 32.65 ± 1.56%, and that for candlenut shells was 41.38 ± 1.94%. The variation in feedstock mass did not result in significant differences in adsorption; the average GNS concentration in coconut was 0.26 ± 0.012 mg/g, and that in candelut was 0.33 ± 0.012 mg/g. However, the use of 300 g of feedstock has optimal absorption of GNS, which is the optimal mass for both feedstocks and may increase the amount of energy available in the system. GNS candlenut is better than coconut in terms of adsorption because there are fewer layers of GNS, which is elaborated by the Raman and XRD analyses in Figures 1 and 2. Many factors affect metal adsorption on graphene. Metal adsorption in graphene differs from other materials due to unique mechanisms, that the adsorb metal ions are influenced by factors like electronegativity, ion charge density, and the presence of an oxygen-based functional group.[77] Furthermore, the surface has a more significant impact on increasing the amount of contact metal with C−π interactions. The adsorption of iron (Fe) onto the GNS in solution involves electron transfer processes that are crucial for understanding the interaction between the two materials. Interestingly, based on the data, Fe adsorbs on graphene via C−π interactions, which are where C−π as partial negative σ^- and Fe as partial

https://doi.org/10.1021/acsomega.4c05745
ACS Omega 2025, 10, 3338−3350

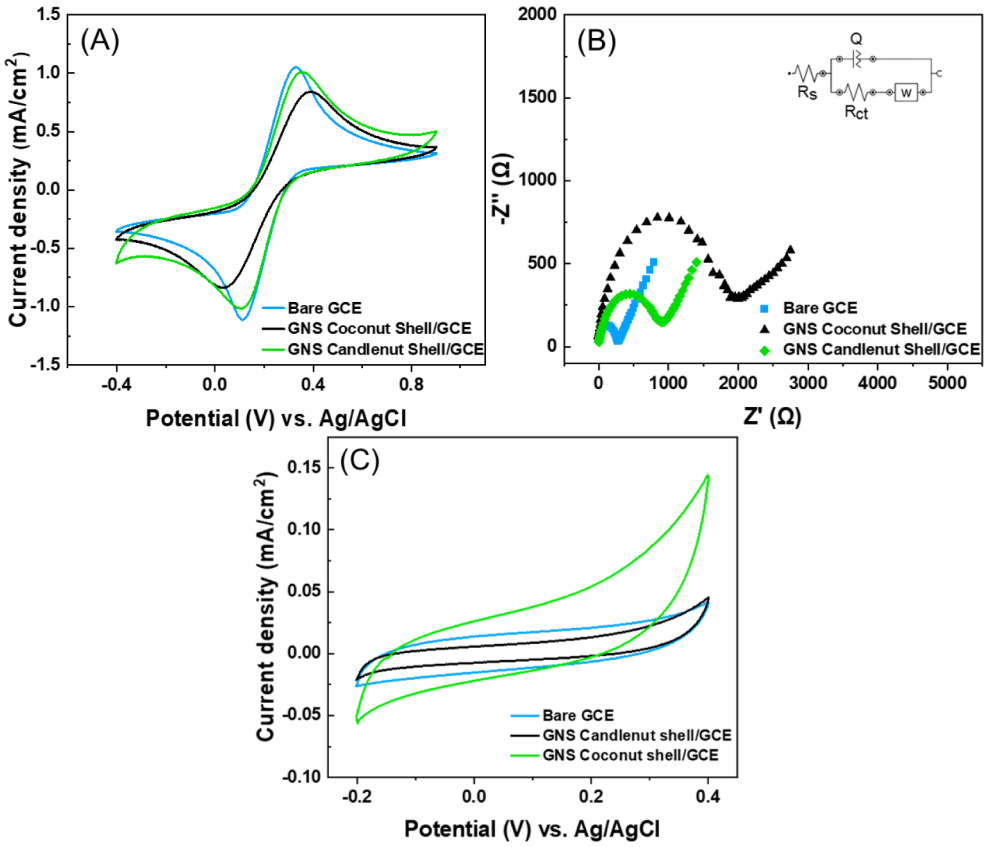

Figure 7. CV curves of the bare GCE and GNS/GCE recorded in 0.1 M KCl containing 5 mM $[Fe(CN)_6]^{3-/4-}$ (A); EIS results of the bare GCE and GNS/GCE recorded in 0.1 M KCl containing 5 mM $[Fe(CN)_6]^{3-/4-}$ (B) and CV curves of the bare GCE, GNS candlenut shell/GCE, and GNS coconut shell/GCE recorded in 1 M KOH at 50 mV/s (C).

positive σ^+, leading to a dipole moment. By stirring the solution, the Fe ions that contact the GNS massively become Fe metal; we assumed that interactive Fe/GNS ((π-d)(Fe-(orbital-s)C−π)) formed ionic bonds. The adsorption of metals on GNS involves a complex interplay; GNS binds Fe physically through surface attraction (van der Waals forces) and chemically by oxidation bonding (chemisorption). From the Fe ion adsorption study, we propose an interaction model of adsorption Fe/GNS. In the first step, Fe compounds are ionized to produce Fe ions; second, when graphene comes into contact with the metal, there can be a redistribution of charge at the interface due to the difference in work functions between the two materials. This charge redistribution can lead to electron transfer from graphene to the metal.[78] C−π interactions with Fe ions change to Fe metal; second, Fe is distributed on GNS; and third, supersaturated Fe metal prevents GNS from absorbing more and releasing Fe metal into the solution.

Electrochemical Analysis. The electrochemical characteristics and electrical conductance of composites fabricated as modified electrodes using graphene-based materials have been examined, revealing the presence of oxidation and reduction peaks corresponding to the redox couple $[Fe(CN)]^{3-}/[Fe(CN)]^{4-}$ shown in Figure 7A. The voltammogram demonstrates the presence of oxide and reduction peaks in the electrochemical response of the modified electrode. CV and EIS analyses were carried out to explain the electrical properties further. Cyclic voltammetry (CV) is a prominent and widely used electrochemical technique that is often used to explore molecular species reduction and oxidation processes. This approach proves invaluable in investigating electron-transfer-initiated chemical reactions, including catalysis. These measurements were carried out in a 0.1 M KCl aqueous solution, which included 5 mM $[Fe(CN)_6]^{3-/4-}$. Moreover, GNS was also conducted using a multimeter and power supply to see the conductivity trend, as shown in Figure S1.

As shown in Figure 7A, $[Fe(CN)^6]^{3-}/[Fe(CN)^6]^{4-}$ redox couples on the bare glassy carbon electrode (GCE) and GCEs modified with GNS derived from coconut and candlenut shells. The redox process observed corresponds to the electrochemical reaction of the ferricyanide/ferrocyanide couple, as presented in eq 3.

$$[Fe(CN)_6]^{3-} + e^- \leftrightarrow [Fe(CN)_6]^{4-} \quad (3)$$

The reaction is affected by the surface properties of the electrode, such as the existence of functional groups, surface imperfections, and the overall conductivity of the electrode surface. The observed peak shifts can be attributed to the disparities in surface characteristics between the GNS-modified electrodes and the bare GCE. GNS obtained from candlenut shells have thinner layers of graphene and fewer imperfections, enabling a more effective transmission of electrons. This is indicated by a decrease in the difference between the peak potentials (ΔEp) and a movement of the oxidation and reduction peaks toward lower potential values, suggesting a more advantageous electron transfer process at the GNS candlenut-modified GCE. On the other hand, the GNS coconut shell-modified GCE, which has thicker layers and more flaws, exhibits a greater ΔEp and peak shifts toward

https://doi.org/10.1021/acsomega.4c05745
ACS Omega 2025, 10, 3338−3350

higher potentials. This indicates a less effective electron transfer process. Based on this curve, it can be concluded that the GCE had a higher peak current and the response of the modified GNS electrodes was poorer than that of the glassy carbon electrode. However, the GNS candlenut shell is better than the GNS coconut shell. Figure 7C shows the measurement scan rates at 50 mV/s and under a stable potential window of −0.2 to 0.4 V. Furthermore, the specific capacitance (Csp) of the GNS electrode can be determined from the galvanostatic charge and discharge using the following eq 4:[79]

$$C_{sp} = \frac{I \mathrm{x} \Delta t}{m \mathrm{x} \Delta V} F/\mathrm{g} \quad (4)$$

where the applied charge−discharge current is represented by I (A), the discharge time by Δt (s), the specific mass of the material by m, and the potential window by ΔV (V). By cycling the modified electrodes in 1 M KOH at 50 mV/s, we calculated the capacitances of the bare GCE (50.4 F/g), candlenut/GCE (108.8 F/g), and coconut/GCE (38.9 F/g) were calculated. The capacitance of the candlenut is better.

These data are in line with those for the layers of GNS; the Raman peak can be interpreted as the ratio of the I_D/I_G number to the high graphitization on the other hand I_{2D}/I_G indicates stacking layers of GNS candlenut slightly fewer layers than coconut, as shown in Figure 1. As the research conducted by Ni et al., the intensity of the 2D band in suspended graphene is affected by charged impurities; the higher ratio I_{2D}/I_G suggests low impurities and higher mobility.[80,81] The electrodes were fitted using a complex equivalent circuit, which models the Nyquist plots using circuit elements. A comparison of the Nyquist plots for the GCE, GNS coconut shell, and GNS candlenut shell is shown in Figure 7B. The use of a small applied potential amplitude and a wide frequency range enables a comprehensive analysis of the electrical behavior of GNS. The Nyquist plot is defined from Randal's equivalent circuit, as shown in the inset of Figure 7B; Rs represents the resistance of the electrolyte, while Q is closely associated with the double-layer capacitance at the interface between the electrode and the liquid electrolyte. W denotes the Warburg resistance, which arises due to ion diffusion in the electrolyte.[82] The charge transfer resistances (Rct) of the bare GCE, candlenut/GCE, and coconut/GCE were 0.30 kΩ, 0.78 kΩ, and 1.94 kΩ, respectively. The CV and electrochemical impedance spectroscopy (EIS) results were consistent. The unmodified GCE shows more electrochemical activity than the GCE treated with GNS since a lower Rct value indicates a more rapid electron transfer rate. Nevertheless, the fact that Rct increased after the graphene-synthesized change suggests that this modification may have created a barrier to electron flow. This might be because of the carbon material's intrinsic physical properties, such as its surface area, porosity, chemical composition, and functional properties.[83] However, sensing, energy storage, and other electrochemical feature-based technologies could benefit from GNS/GCE's increased efficiency in terms of current density and peak precision.

CONCLUSIONS

The aforementioned conclusions were derived from the outcomes and subsequent analysis of the preceding studies. GNS was effectively produced from coconut and candlenut shells using a pyrolysis technique, showcasing its potential as a sustainable and efficient method for large-scale manufacturing from candlenut and coconut shells. GNS verified the structural characteristics, flaws, and elemental makeup of the produced GNS. The GNS showed a significant ability to adsorb Fe ions, achieving adsorption efficiencies of approximately 32.65% for GNS obtained from coconut shells and 41.38% for GNS derived from candlenut shells. The adsorption mechanism entails an intricate combination of physical and chemical interactions, such as C-π interactions and surface adsorption, resulting in the reduction of Fe ions to Fe metal on the GNS surface. The observations led to the proposal of an interaction model between Fe ions and GNS. This model emphasizes the important steps in the adsorption process, mechanisms of electron transfer, and production of Fe metal on the GNS surface. The electrodes treated with GNS showed alterations in their electrochemical activity, displaying different charge transfer resistances (Rct) in comparison with the unmodified electrodes. These findings indicate that GNS-modified electrodes have the potential to be used in electrochemical sensing and energy storage systems. Potential areas for future research could involve refining the synthesis settings. This study enhances our comprehension of the production and modification of graphene nanosheets derived from biomass waste as well as their potential utilization in several domains. It establishes a solid foundation for future progress in the disciplines of materials science and nanotechnology.

METHODOLOGY

Materials. Coconut fruits of the *Cocos nucifera L.* and candlenut shells of the *Aleurites moluccana L.* Wild varieties were provided by a local farmer. Aluminum foil, $(NH_4)_2Fe(SO_4)_2.6H_2O$ (99%), H_2SO_4 (≥99.9%), HNO_3 (≥90%), activated charcoal (AC) powder, deionized (DI) water, Whatman qualitative filter paper grade 1, and 96% pure graphene were obtained from Sigma−Aldrich, USA.

Producing Biocharcoal. Candlenut shells were cleaned of attached fibers, wrapped with aluminum foil, and placed on top of the heater for 20 min. Then, the shell was separated from the fibers, dried again, and heated in an argon atmosphere at 600 °C for 5 h. Then, the charcoal is cleaned from ash to produce solid black charcoal

Producing GNS. The synthesized GNS were made by the pyrolysis of charcoal-like graphene oxide, which is a reduction oxide group, using AC to produce GNS through pyrolysis under Ag atmosphere at 0.8 mbar and 600 °C. The mixture of AC and GNS was separated by washing the sample using DI water, dried in a vacuum oven at 80 °C for 12 hours, and then ground into powder with 200 mesh schematic process shown in Figure 8A. The sample XRD was used to confirm the transformation of the crystal structure (Figure 8B−D)

Sample Characterization. The GNS were analyzed via Raman spectroscopy (Renishaw inVia confocal Raman microscope (UK)), X-ray diffraction (XRD) with a Cu/Kα radiation monochromator (α = 1.5406) at 40 kV (Rigaku Corporation, Japan), and field emission scanning electron microscopy (FESEM) with an energy dispersive X-ray system (JEOL JSM-7600F, Japan). A total of 20 kV for energy dispersive spectroscopy (EDS) and 5 kV for imaging were used, and a transmission electron microscope (JEOL 2100F, Japan) and a Fourier transform infrared (FTIR) instrument (Agilent Cary 630 FTIR, USA) were used.

Fe Adsorption Analysis. Metal adsorption analysis Fe measurements were performed using a single beam, Czerny-Turner design grating monochromator with a measurement range of 190−900 nm, a graphite furnace flame atomic

https://doi.org/10.1021/acsomega.4c05745
ACS Omega 2025, 10, 3338−3350

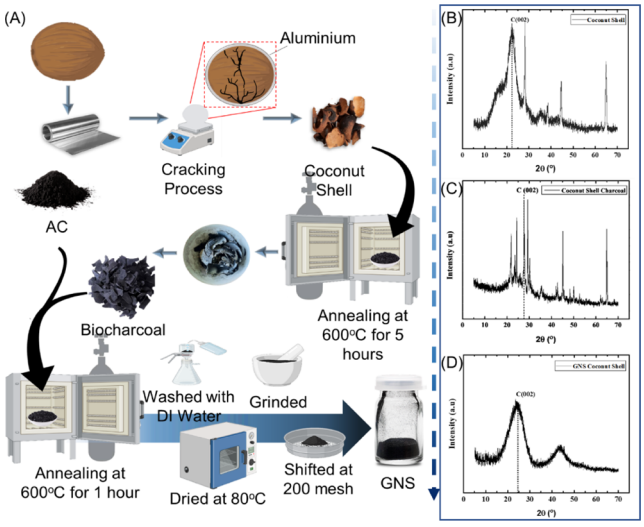

Figure 8. Schematic of the GNS synthesis process (A); XRD patterns of coconut shell (B); coconut shell charcoal (C) reprinted with permission from ref[84] Copyright 2020 Scitepress and GNS coconut shell (D).

absorption spectroscopy (AAS) instrument DW-200 DRA-WELL spectrophotometer (China) and iron standards of 0 ppm, 1, 3, 5, 6, 7, 8, 9, and 10 ppm, and the following equation was used: y = 0.065372 Conc + 0.035081, as shown in Figure S2B. A total of 0.5 g of GNS samples from coconut shells and hazelnut shells were put into a glass beaker that contained a standard 4.0 ppm iron solution. The magnetic bar was placed in a glass beaker and stirred for 70 min. Subsequently, the solution was filtered using Whatman filter paper.

In our study, depicted in (Figure S2A), we investigated the adsorption process, and a full adsorption experiment using a regular iron solution was carried out. To create the acidic environment we needed for our work, H_2SO_4 was added to deionized (DI) water. This made it easier for $(NH_4)_2Fe(SO_4)_2.6H_2O$ to dissolve. This step was very important for getting the medium ready for the next responses. Then, $KMnO_4$ was slowly added to start oxidation reactions that changed Fe(III) ions to Fe(II) ions, which are important building blocks for the next reduction step. When these ions intercalated into the GNS, they were reduced to elemental Fe(0), which showed that our adsorption mechanism worked. After this reaction phase, the filtrate was carefully sorted, which allowed us to measure our results accurately. Using atomic absorption spectroscopy (AAS) instruments, we measured the absorbance at λmax = 248.3 nm, which is a good way to tell how much Fe metal is in it. The precise measurements that led to this absorbance value were used to figure out the final concentration of Fe in the sample. To make sure our results were solid, we made GNS samples with different amounts of fuel and measured them five times to make sure they were accurate and reliable when testing Fe metal adsorption. We used a special equation, eq 5, to measure how well our adsorption process worked. This showed how the GNS properties and the Fe metal adsorption efficiency are connected in a complex way.[85]

$$W = \frac{(C_o - C_e)}{W_a} \times V \quad (5)$$

where W is the adsorption capacity at equilibrium ($mg.g^{-1}$), C_o is the initial concentration (mgL^{-1}), C_e is the concentration at equilibrium (mgL^{-1}), W_a is the amount of adsorbent (g), and V is the volume of solution (L).

Electrochemistry Analysis. Electrochemical measurements were conducted using a Potentiostat/Galvanostat Autolab PGSTAT30, Eco-chemie (Netherlands) within a three-electrode system. The electrochemical cells consisted of a modified glassy carbon working electrode (GCE, diameter of 3 mm), a Ag/AgCl reference electrode, and a platinum rod counter electrode.

The glassy carbon electrode (GCE) was polished using alumina powder and washed extensively with distilled water before being employed. A homogenized suspension of 1 mg/mL GNS was prepared by dispersing the synthesized GNS in distilled water through ultrasonication for 30 min. Subsequently, 5 μL of this suspension was drop-casted onto the surface of the GCE and allowed to air-dry at room temperature, resulting in the formation of GNS/GCE.[86]

■ ASSOCIATED CONTENT

Data Availability Statement

The authors declare that the data supporting the findings of this study are available within the paper and its Supporting Information files.

Supporting Information

The Supporting Information is available free of charge at https://pubs.acs.org/doi/10.1021/acsomega.4c05745.

Percent product yield; conductivity measurement using a multimeter and power supply (PDF)

■ AUTHOR INFORMATION

Corresponding Author

Rikson Siburian − *Carbon and Frankincense Research Center, Universitas Sumatera Utara, Medan 20155, Indonesia; Department of Chemistry, Faculty of Mathematics and Natural Sciences, Universitas Sumatera Utara, Medan 20155, Indonesia*; Email: rikson@usu.ac.id

Authors

Yosia Gopas Oetama Manik − *Department of Postgraduate of Chemistry, Faculty of Mathematics and Natural Sciences and Department of Chemistry, Faculty of Mathematics and Natural Sciences, Universitas Sumatera Utara, Medan 20155, Indonesia; Carbon and Frankincense Research Center, Universitas Sumatera Utara, Medan 20155, Indonesia*

Boon Tong Goh − *Low Dimensional Materials Research Centre, Department of Physics, Faculty of Science, University of Malaya, Kuala Lumpur 50603, Malaysia*; orcid.org/0000-0003-3933-7594

Yatimah Alias − *University Malaya Centre for Ionic Liquids (UMCiL) and Department of Chemistry, Faculty of Science, Universiti Malaya, Kuala Lumpur 50603, Malaysia*

Complete contact information is available at: https://pubs.acs.org/10.1021/acsomega.4c05745

Author Contributions

Y.G.O.M.: Conceptualization, Methodology, Formal analysis, Project administration, Investigation, Writing—Original Draft; B.T.G.: Conceptualization, Validation, Methodology, Writing—Review and Editing; R.S.: Conceptualization, Super-

https://doi.org/10.1021/acsomega.4c05745
ACS Omega 2025, 10, 3338−3350

vision, Funding acquisition, Writing—Review and Editing. All authors contributed to the final manuscript; Y.A.: Validation, Methodology, Writing—Review and Editing.

Notes

The authors declare no competing financial interest.

■ ACKNOWLEDGMENTS

The authors would like to thank for financial support from Direktorat Jenderal Pendidikan Tinggi, Riset dan Teknologi Republik Indonesia tahun 2024 with contract number 82/UN5.4.10.S/PPM/KP-DRPTM/2024 through the DRPTM Project, TALENTA Program HIBAH PENELITIAN TERAPAN 2021 No. 2052/UN5.1.R/SK/PPM/2021 and this work was supported by EQUITY Project released by the Ministry of Higher Education, Culture, Research, and Technology of Republic of Indonesia (Grant No. 59/E/HK.02.02/2022), LPDP-Indonesia Endowment Fund for Education Agency of the Ministry of Finance of Republic of Indonesia (Grant No. RJP-24/LPDP/2022), Directorate General of Higher Education, Research, and Technology (Grant No. 3792/E3/DT.03.08/2023), and Universitas Sumatera Utara (Grant No. 8154.1/UN5.1.R/KPM/2023)

■ ABBREVIATIONS

GNS, Graphene Nano Sheets; CV, Cyclic Voltammetry; EIS, electrochemical impedance spectroscopy; GCE, Glassy Carbon Electrode; fwhm, Full width at half-maximum; Rct, Resistances charge transfer; Rs, Resistance of the electrolyte

■ REFERENCES

(1) Aval, L. F.; Ghoranneviss, M.; Pour, G. B. High-Performance Supercapacitors Based on the Carbon Nanotubes, Graphene and Graphite Nanoparticles Electrodes. *Heliyon* **2018**, *4* (11), No. e00862.
(2) Siburian, R.; Paiman, S.; Hutagalung, F.; Marwan Ali, A. M.; Simatupang, L.; Goei, R.; Rusop, M. M. Developing Nickel/Graphene Nano Sheets as an Alternative Primary Battery Anode. *Ceram. Int.* **2022**, *48* (9), 12897−12905.
(3) Siburian, R.; Goei, R.; Manurung, H.; Aritonang, S. P.; Simanjuntak, C.; Hutagalung, F.; Anshori, I.; Alias, Y.; Paiman, S.; Affi, J.; Tok, A. I. Y. Distribution Model of Iron (Fe) on Fe/Graphene Nano Sheets. *Ceram. Int.* **2023**, *49* (17), 28571−28579.
(4) Simanjuntak, C.; Siburian, R.; Marpaung, H.; Tamrin. Properties of Mg/Graphite and Mg/Graphene as Cathode Electrode on Primary Cell Battery. *Heliyon* **2020**, *6* (1), No. e03118.
(5) Saeed, M.; Alshammari, Y.; Majeed, S. A.; Al-Nasrallah, E. Chemical Vapour Deposition of Graphene—Synthesis, Characterisation, and Applications: A Review. *Molecules* **2020**, *25* (17), 3856.
(6) Laref, A.; Alsagri, M.; Alay-E-Abbas, S. M.; Barakat, F.; Laref, S.; Huang, H. M.; Xiong, Y. C.; Yang, J. T.; Wu, X. Impact of Phosphorous and Sulphur Substitution on Dirac Cone Modification and Optical Behaviors of Monolayer Graphene for Nano-Electronic Devices. *Appl. Surf. Sci.* **2019**, *489*, 358−371.
(7) Kota, M.; Park, H. S. Restacking-Inhibited Nitrogen-Incorporated Mesoporous Reduced Graphene Oxides for High Energy Supercapacitors. *Ceram. Int.* **2018**, *44* (3), 3195−3200.
(8) Carraro, G.; Savio, L.; Vattuone, L. Influence of Defects and Heteroatoms on the Chemical Properties of Supported Graphene Layers. *Coatings* **2022**, *12* (3), 397.
(9) Han, Y.; Fang, Y.; Ding, X.; Liu, J.; Jin, Z.; Xu, Y. A Simple and Effective Flexible Electrochemiluminescence Sensor for Lidocaine Detection. *Electrochem. Commun.* **2020**, *116*, 106760.
(10) Mbayachi, V. B.; Ndayiragije, E.; Sammani, T.; Taj, S.; Mbuta, E. R.; Khan, A. U. Graphene Synthesis, Characterization and Its Applications: A Review. *Results Chem.* **2021**, *3*, 100163.
(11) Cebadero-Dominguez, Ó.; Casas-Rodríguez, A.; Puerto, M.; Cameán, A. M.; Jos, A. In Vitro Safety Assessment of Reduced Graphene Oxide in Human Monocytes and T Cells. *Environ. Res.* **2023**, *232*, 116356.
(12) Robinson, C.; Juska, V. B.; O'Riordan, A. Surface Chemistry Applications and Development of Immunosensors Using Electrochemical Impedance Spectroscopy: A Comprehensive Review. *Environ. Res.* **2023**, *237*, 116877.
(13) Baqiya, M. A.; Nugraheni, A. Y.; Islamiyah, W.; Kurniawan, A. F.; Ramli, M. M.; Yamaguchi, S.; Furukawa, Y.; Soontaranon, S.; Putra, E. G. R.; Cahyono, Y.; et al. Structural study on graphene-based particles prepared from old coconut shell by acid−assisted mechanical exfoliation. *Adv. Powder Technol.* **2020**, *31* (5), 2072−2078.
(14) Abbas, A.; Eng, X. E.; Ee, N.; Saleem, F.; Wu, D.; Chen, W.; Handayani, M.; Tabish, T. A.; Wai, N.; Lim, T. M. Development of Reduced Graphene Oxide from Biowaste as an Electrode Material for Vanadium Redox Flow Battery. *J. Energy Storage* **2021**, *41*, 102848.
(15) Ismail, M. S.; Yusof, N.; Mohd Yusop, M. Z.; Ismail, A. F.; Jaafar, J.; Aziz, F.; Abdul Karim, Z. Synthesis and Characterization of Graphene Derived from Rice Husks. *Malaysian J. Fundam. Appl. Sci.* **2019**, *15* (4), 516−521.
(16) Munuera, J.; Britnell, L.; Santoro, C.; Cuéllar-Franca, R.; Casiraghi, C. A Review on Sustainable Production of Graphene and Related Life Cycle Assessment. *2D Mater.* **2022**, *9* (1), 012002.
(17) Huang, M.; Ruoff, R. S. Growth of Single-Layer and Multilayer Graphene on Cu/Ni Alloy Substrates. *Acc. Chem. Res.* **2020**, *53* (4), 800−811.
(18) Pei, S.; Wei, Q.; Huang, K.; Cheng, H. M.; Ren, W. Green Synthesis of Graphene Oxide by Seconds Timescale Water Electrolytic Oxidation. *Nat. Commun.* **2018**, *9* (1), 145.
(19) Luo, Y.; Barwa, T. N.; Dempsey, E.; Karthik, R.; Shim, J. J.; Sukanya, R.; Breslin, C. B. Electrochemical Detection of Sulfanilamide Using Tannic Acid Exfoliated MoS2 Nanosheets Combined with Reduced Graphene Oxide/Graphite. *Environ. Res.* **2024**, *248*, 118391.
(20) Siburian, R.; Ali, A. M. M.; Sebayang, K.; Supeno, M.; Tarigan, K.; Simanjuntak, C.; Aritonang, S. P.; Hutagalung, F. The Loading Effect of Pt Clusters on Pt/Graphene Nano Sheets Catalysts. *Sci. Rep.* **2021**, *11* (1), 2532.
(21) Bu, Y.; Guo, F.; Li, K.; Liang, Z.; Zhang, J.; Jiang, C.; Bi, Z. High-Temperature Pyrolysis Behavior and Structural Evolution Mechanism of Graphene Oxide: A ReaxFF Molecular Dynamics Simulation. *Appl. Surf. Sci.* **2022**, *593*, 153451.
(22) Siburian, R.; Tang, L. W.; Alias, Y.; Tok, A. I. Y.; Goei, R.; Simanjuntak, C.; Tarigan, K.; Paiman, S.; Goh, B. T.; Anshori, I.; Kurniawan, C. Coconut Waste to Green Nanomaterial: Large Scale Synthesis of N-Doped Graphene Nano Sheets. *Nano-Struct. Nano-Objects* **2023**, *36*, 101061.
(23) Zhang, C.; Tan, J.; Pan, Y.; Cai, X.; Zou, X.; Cheng, H. M.; Liu, B. Mass Production of 2D Materials by Intermediate-Assisted Grinding Exfoliation. *Natl. Sci. Rev.* **2020**, *7* (2), 324−332.
(24) Wu, Y.; Yuan, Y.; Shuang, W.; Wang, L.; Yang, L.; Bai, Z.; Lu, J. Reducing Carbonaceous Salts for Facile Fabrication of Monolayer Graphene. *Small Methods* **2023**, *7* (3), 2201596.
(25) Chen, J.; Li, L. Effect of Oxidation Degree on the Thermal Properties of Graphene Oxide. *J. Mater. Res. Technol.* **2020**, *9* (6), 13740−13748.
(26) Kim, M. S.; Kim, K. J.; Kim, M.; Lee, S.; Lee, K. H.; Kim, H.; Kim, H. M.; Kim, K. B. Cu Oxidation Kinetics through Graphene and Its Effect on the Electrical Properties of Graphene. *RSC Adv.* **2020**, *10* (59), 35671−35680.
(27) Lanza, M.; Wang, Y.; Gao, T.; Bayerl, A.; Porti, M.; Nafria, M.; Zhou, Y.; Jing, G.; Zhang, Y.; Liu, Z.; Yu, D.; Duan, H. Electrical and Mechanical Performance of Graphene Sheets Exposed to Oxidative Environments. *Nano Res.* **2013**, *6* (7), 485−495.
(28) Kozodaev, M. G.; Slavich, A. S.; Romanov, R. I.; Zarubin, S. S.; Markeev, A. M. Influence of Reducing Agent on Properties of Thin WS2 Nanosheets Prepared by Sulfurization of Atomic Layer-Deposited WO3. *J. Phys. Chem. C* **2020**, *124* (51), 28169−28177.

https://doi.org/10.1021/acsomega.4c05745
ACS Omega 2025, 10, 3338−3350

(29) Lesiak, B.; Trykowski, G.; Tóth, J.; Biniak, S.; Kövér, L.; Rangam, N.; Stobinski, L.; Malolepszy, A. Chemical and Structural Properties of Reduced Graphene Oxide—Dependence on the Reducing Agent. *J. Mater. Sci.* **2021**, *56* (5), 3738−3754.
(30) Zergui, A.; Joseph, M. L.; Inkale, C. B. ICP-MS Assessment of Elemental Impurities and Metallic Contaminants in Activated Charcoal Products. *BioMetals* **2023**, *36* (5), 969−974.
(31) Zhang, B.; Jiang, Y.; Balasubramanian, R. Synthesis, Formation Mechanisms and Applications of Biomass-Derived Carbonaceous Materials: A Critical Review. *J. Mater. Chem. A* **2021**, *9* (44), 24759−24802.
(32) Ahmad Farid, M. A.; Andou, Y. A Route towards Graphene from Lignocellulosic Biomass: Technicality, Challenges, and Their Prospective Applications. *J. Cleaner Prod.* **2022**, *380*, 135090.
(33) Mariana, M.; Mistar, E. M.; Syabriyana, M.; Zulkipli, A. S.; Aswita, D.; Alfatah, T. Properties and Adsorptive Performance of Candlenut Shell and Its Porous Charcoals for Aqueous Mercury(II) Removal. *Bioresour. Technol. Rep.* **2022**, *19*, 101182.
(34) Tamilselvi, R.; Ramesh, M.; Lekshmi, G. S.; Bazaka, O.; Levchenko, I.; Bazaka, K.; Mandhakini, M. Graphene Oxide − Based Supercapacitors from Agricultural Wastes: A Step to Mass Production of Highly Efficient Electrodes for Electrical Transportation Systems. *Renewable Energy* **2020**, *151*, 731−739.
(35) Siburian, R.; Tarigan, K.; Manik, Y. G. O.; Hutagalung, F.; Alias, Y.; Chan, Y. C.; Chang, B. P.; Siow, J.; Ong, A. J.; Huang, J.; et al. Converting Candlenut Shell Waste into Graphene for Electrode Applications. *Processes* **2024**, *12* (8), 1544.
(36) Plenča, K.; Cvetnić, S.; Prskalo, H.; Kovačić, M.; Cvetnić, M.; Kušić, H.; Matusinović, Z.; Kraljić Roković, M.; Genorio, B.; Lavrenčič Štangar, U.; et al. Biomass Pyrolysis-Derived Biochar: A Versatile Precursor for Graphene Synthesis. *Materials* **2023**, *16* (24), 7658.
(37) Schmidt, S. J.; Dou, W.; Sydlik, S. A. Regeneratable Graphene-Based Water Filters for Heavy Metal Removal at Home. *ACS EST Water* **2023**, *3*, 2179−2185.
(38) Kim, M. S.; Lee, J.; Kim, H. S.; Cho, A.; Shim, K. H.; Le, T. N.; An, S. S. A.; Han, J. W.; Kim, M., Il; Lee, J. Heme Cofactor-Resembling Fe−N Single Site Embedded Graphene as Nanozymes to Selectively Detect H2O2 with High Sensitivity. *Adv. Funct. Mater.* **2020**, *30* (1), 1905410.
(39) Li, Y.-M.; Nishidate, K. Unravelling the Micro-Mechanism of Oxygen Reduction Reaction on Fe−N4 Embedded in Graphene. *Int. J. Hydrogen Energy* **2024**, *51*, 1471−1475.
(40) Azad, D.; Pateriya, R. N.; Sharma, R. K. Chemical Activation of Pine Needle and Coconut Shell Biochar: Production, Characterization and Process Optimization. *Int. J. Environ. Sci. Technol.* **2024**, *21*, 757−772.
(41) Wibisono, Y.; Firdayanti, N.; Salsabila, G. N.; Rafianto, V.; Alvianto, D.; Dewi, S. R.; Hawa, L. C. Preparation of Activated Carbon From Local Biowaste As Fillers For Mixed Matrix Membranes. *Brawijaya International Conference*; Atlantis Press, 2023, *2*, 517−528.
(42) Supeno, M.; Siburian, R. New Route: Convertion of Coconut Shell Tobe Graphite and Graphene Nano Sheets. *J. King Saud Univ. −Sci.* **2020**, *32* (1), 189−190.
(43) Teng, T. P.; Chang, S. C.; Chen, Z. Y.; Huang, C. K.; Tseng, S. F.; Yang, C. R. High-Yield Production of Graphene Flakes Using a Novel Electrochemical/Mechanical Hybrid Exfoliation. *Int. J. Adv. Manuf. Technol.* **2019**, *104* (5−8), 2751−2760.
(44) Ojrzyńska, M.; Daniewski, A. R.; Wilczyński, K.; Jamroz, J.; Dużyńska, A.; Zdrojek, M. High-Quality Graphene Nanoplatelets Production with 100% Yield Based on Popular Fertilizer Industry Feedstock. *J. Phys. Chem. C* **2024**, *128* (1), 516−524.
(45) Tan, H.; Navik, R.; Liu, Z.; Xiang, Q.; Zhao, Y. Scalable Massive Production of Defect-Free Few-Layer Graphene by Ball-Milling in Series with Shearing Exfoliation in Supercritical CO2. *J. Supercrit. Fluids* **2022**, *181*, 105496.
(46) van der Zee, L. J. C.; Hofman, J.; van Gaalen, J. M.; Slootweg, J. C. Mechanistic Studies on Single-Electron Transfer in Frustrated Lewis Pairs and Its Application to Main-Group Chemistry. *Chem. Soc. Rev.* **2024**, *53* (10), 4862−4876.
(47) Ong, H. C.; Chen, W. H.; Singh, Y.; Gan, Y. Y.; Chen, C. Y.; Show, P. L. A State-of-the-Art Review on Thermochemical Conversion of Biomass for Biofuel Production: A TG-FTIR Approach. *Energy Convers. Manage.* **2020**, *209*, 112634.
(48) Li, S.; Galoustian, T.; Trejo, H. Journal of Analytical and Applied Pyrolysis Biochar Pyrolyzed with Concentrated Solar Radiation for Enhanced Nitrate Adsorption. *J. Anal. Appl. Pyrolysis.* **2023**, *174*, 106131.
(49) Abdullah, M. A.; Albarody, T. M. B.; Hussein, A. R. Graphite Thermal Expansion Coefficient Measured by In-Situ x-Ray Diffraction. *Nanotechnology* **2020**, *31* (28), 285709.
(50) Zhang, X.; Huo, L.; Yao, Z.; Xie, T.; Jia, J.; Sun, Y.; Zhao, Y.; Zhao, L. Pyrolysis Characteristics and Hydrogen Production Mechanism of Biomass Impregnated with Transition Metals. *J. Clean. Prod.* **2024**, *474*, 143572.
(51) Saha, S.; Lakhe, P.; Mason, M. J.; Coleman, B. J.; Arole, K.; Zhao, X.; Yakovlev, S.; Uppili, S.; Green, M. J.; Hule, R. A. Sustainable Production of Graphene from Petroleum Coke Using Electrochemical Exfoliation. *Npj 2D Mater. Appl* **2021**, *5* (1), 75.
(52) Roscher, S.; Hoffmann, R.; Ambacher, O. Determination of the Graphene-Graphite Ratio of Graphene Powder by Raman 2D Band Symmetry Analysis. *Anal. Methods* **2019**, *11* (9), 1180−1191.
(53) Alkhouzaam, A.; Qiblawey, H.; Khraisheh, M.; Atieh, M.; Al-Ghouti, M. Synthesis of Graphene Oxides Particle of High Oxidation Degree Using a Modified Hummers Method. *Ceram. Int.* **2020**, *46* (15), 23997−24007.
(54) Payandehpeyman, J.; Mazaheri, M.; Khamehchi, M. Prediction of Electrical Conductivity of Polymer-Graphene Nanocomposites by Developing an Analytical Model Considering Interphase, Tunneling and Geometry Effects. *Compos. Commun.* **2020**, *21*, 100364.
(55) López-Díaz, D.; Delgado-Notario, J. A.; Clericò, V.; Diez, E.; Merchán, M. D.; Velázquez, M. M. Towards Understanding the Raman Spectrum of Graphene Oxide: The Effect of the Chemical Composition. *Coatings* **2020**, *10* (6), 524.
(56) Wu, J.; Yang, Y.; Qu, Y.; Jia, L.; Zhang, Y.; Xu, X.; Chu, S. T.; Little, B. E.; Morandotti, R.; Jia, B.; et al. 2D Layered Graphene Oxide Films Integrated with Micro-Ring Resonators for Enhanced Nonlinear Optics. *Small* **2020**, *16* (16), 1906563.
(57) Sulaiman, S.; Sudin, I.; Al-Naib, U. M. B.; Omar, M. F. Review of the Nanostructuring and Doping Strategies for High-Performance ZnO Thermoelectric Materials. *Crystals* **2022**, *12* (8), 1076.
(58) Sim, H. J.; Li, Z.; Xiao, P.; Lu, H. The Influence of Lateral Size and Oxidation of Graphene Oxide on Its Chemical Reduction and Electrical Conductivity of Reduced Graphene Oxide. *Molecules* **2022**, *27* (22), 7840.
(59) Silva, D. L.; Campos, J. L. E.; Fernandes, T. F. D.; Rocha, J. N.; Machado, L. R. P.; Soares, E. M.; Miquita, D. R.; Miranda, H.; Rabelo, C.; Vilela Neto, O. P.; Jorio, A.; Cançado, L. G. Raman Spectroscopy Analysis of Number of Layers in Mass-Produced Graphene Flakes. *Carbon* **2020**, *161*, 181−189.
(60) Nor, N. H. M.; Anuar, N. A.; Talik, N. A.; Wan Abdullah, W. A. T.; Kittimanapun, K.; Nakajima, H.; Chanlek, N.; Yahya, M. F. Z. R.; Goh, B. T. Effects of High-Energy Electron Beam Irradiation on the Structure, Composition and Morphological Properties of Graphene Nanoplatelet Films. *Sains Malays* **2023**, *52* (10), 2955−2970.
(61) Anuar, N. A. B.; Nor, N. H. M.; Awang, R. B.; Nakajima, H.; Tunmee, S.; Tripathi, M.; Dalton, A.; Goh, B. T. Low-Temperature Growth of Graphene Nanoplatelets by Hot-Wire Chemical Vapour Deposition. *Surf. Coat. Technol.* **2021**, *411*, 126995.
(62) Papanai, G. S.; Sharma, I.; Gupta, B. K. Probing Number of Layers and Quality Assessment of Mechanically Exfoliated Graphene via Raman Fingerprint. *Mater. Today Commun.* **2020**, *22*, 100795.
(63) Jaworski, S.; Wierzbicki, M.; Sawosz, E.; Jung, A.; Gielerak, G.; Biernat, J.; Jaremek, H.; Łojkowski, W.; Woźniak, B.; Wojnarowicz, J.; et al. Graphene Oxide-Based Nanocomposites Decorated with Silver Nanoparticles as an Antibacterial Agent. *Nanoscale Res. Lett.* **2018**, *13* (1), 116.

https://doi.org/10.1021/acsomega.4c05745
ACS Omega 2025, 10, 3338−3350

(64) Haidari, M. M.; Kim, H.; Kim, J. H.; Park, M.; Lee, H.; Choi, J. S. Doping Effect in Graphene-Graphene Oxide Interlayer. *Sci. Rep.* **2020**, *10* (1), 8258.
(65) Ristiani, D.; Asih, R.; Astuti, F.; Baqiya, M. A.; Kaewhan, C.; Tunmee, S.; Nakajima, H.; Soontaranon, S.; Darminto. Mesostructural Study on Graphenic-Based Carbon Prepared from Coconut Shells by Heat Treatment and Liquid Exfoliation. *Heliyon* **2022**, *8* (3), No. e09032.
(66) Wu, W.; Liu, J.; Li, X.; Hua, T.; Cong, X.; Chen, Z.; Ying, F.; Shen, W.; Lu, B.; Dou, K.; Zhou, X. Incorporation Graphene into Sprayed Epoxy−Polyamide Coating on Carbon Steel: Corrosion Resistance Properties. *Corros. Eng., Sci. Technol.* **2018**, *53* (8), 625−632.
(67) Krawezyk, P.; Gurzeda, B.; Bachar, A. Thermal Exfoliation of Electrochemically Obtained Graphitic Materials. *Appl. Surf. Sci.* **2019**, *481*, 466−472.
(68) Pandey, S.; Karakoti, M.; Surana, K.; Dhapola, P. S.; SanthiBhushan, B.; Ganguly, S.; Singh, P. K.; Abbas, A.; Srivastava, A.; Sahoo, N. G. Graphene Nanosheets Derived from Plastic Waste for the Application of DSSCs and Supercapacitors. *Sci. Rep.* **2021**, *11* (1), 1−17.
(69) Lee, S.; Nathan, A.; Alexander-Webber, J.; Braeuninger-Weimer, P.; Sagade, A. A.; Lu, H.; Hasko, D.; Robertson, J.; Hofmann, S. Dirac-Point Shift by Carrier Injection Barrier in Graphene Field-Effect Transistor Operation at Room Temperature. *ACS Appl. Mater. Interfaces* **2018**, *10* (13), 10618−10621.
(70) Díez, D.; Urueña, A.; Piñero, R.; Barrio, A.; Tamminen, T. Determination of Hemicellulose, Cellulose, and Lignin Content in Different Types of Biomasses by Thermogravimetric Analysis and Pseudocomponent Kinetic Model (TGA-PKM Method). *Processes* **2020**, *8* (1048), 1048.
(71) Das, P.; Deoghare, A. B.; Maity, S. R. A Novel Approach to Synthesize Reduced Graphene Oxide (RGO) at Low Thermal Conditions. *Arab. J. Sci. Eng.* **2021**, *46* (6), 5467−5475.
(72) Kabir Ahmad, R.; Anwar Sulaiman, S.; Yusup, S.; Sham Dol, S.; Inayat, M.; Aminu Umar, H. Exploring the Potential of Coconut Shell Biomass for Charcoal Production. *Ain Shams Eng. J.* **2022**, *13* (1), 101499.
(73) Chen, W. H.; Eng, C. F.; Lin, Y. Y.; Bach, Q. V. Independent Parallel Pyrolysis Kinetics of Cellulose, Hemicelluloses and Lignin at Various Heating Rates Analyzed by Evolutionary Computation. *Energy Convers. Manage.* **2020**, *221*, 113165.
(74) Zhao, L.; Luo, G.; Cheng, Y.; Li, X.; Zhou, S.; Luo, C.; Wang, J.; Liao, H. G.; Golberg, D.; Wang, M. S. Shaping and Edge Engineering of Few-Layered Freestanding Graphene Sheets in a Transmission Electron Microscope. *Nano Lett.* **2020**, *20* (4), 2279−2287.
(75) Torres, F. G.; Troncoso, O. P.; Rodriguez, L.; De-la-Torre, G. E. Sustainable Synthesis, Reduction and Applications of Graphene Obtained from Renewable Resources. *Sustain. Mater. Technol.* **2021**, *29* (June), No. e00310.
(76) Papasouli, E.; Otero, N.; Desmarais, J.; Denawi, H.; Xenides, D.; Klontzas, E.; Koukaras, E. N.; Karamanis, P. On the Optical Properties of Diamino-Pillared Graphene Architectures. *J. Phys. Chem. C* **2023**, *127* (14), 6959−6973.
(77) Malhotra, M.; Puglia, M.; Kalluri, A.; Chowdhury, D.; Kumar, C. V. Adsorption of Metal Ions on Graphene Sheet for Applications in Environmental Sensing and Wastewater Treatment. *Sens. Actuators Rep.* **2022**, *4*, 100077.
(78) Rahmani, M.; Ghafoorifard, H.; Ahmadi, M. T. A Phenomenological Model for Electrical Transport Characteristics of MSM Contacts Based on GNS. *Micromachines* **2023**, *14* (1), 184.
(79) Thirumal, V.; Sreekanth, T. V. M.; Yoo, K.; Kim, J. Facile Preparations of Electrochemically Exfoliated N-Doped Graphene Nanosheets from Spent Zn-Carbon Primary Batteries Recycled for Supercapacitors Using Natural Sea Water Electrolytes. *Energies* **2022**, *15* (22), 8650.
(80) Ni, Z. H.; Yu, T.; Luo, Z. Q.; Wang, Y. Y.; Liu, L.; Wong, C. P.; Miao, J.; Huang, W.; Shen, Z. X. Probing Charged Impurities in Suspended Graphene Using Raman Spectroscopy. *ACS Nano* **2009**, *3* (3), 569−574.
(81) Suszalski, D.; Rut, G.; Rycerz, A. Conductivity Scaling and the Effects of Symmetry-Breaking Terms in Bilayer Graphene Hamiltonian. *Phys. Rev. B* **2020**, *101* (12), 125425.
(82) Tziviloglou, E.; Metaxa, Z. S.; Maistros, G.; Kourkoulis, S. K.; Karousos, D. S.; Favvas, E. P.; Alexopoulos, N. D. Electrochemical Impedance as an Assessment Tool for the Investigation of the Physical and Mechanical Properties of Graphene-Based Cementitious Nanocomposites. *Nanomaterials* **2023**, *13* (19), 2652.
(83) Prasankumar, T.; Jose, S.; Ajayan, P. M.; Ashokkumar, M. Functional Carbons for Energy Applications. *Mater. Res. Bull.* **2021**, *142*, 111425.
(84) Supeno, M.; Siburian, R.; Natalia, D. *The Synthesis of Graphene from Coconut Shell Charcoal*; Science and Technology Publication, 2020; pp. 39−44.
(85) Das, P.; Ibrahim, S.; Chakraborty, K.; Ghosh, S.; Pal, T. Stepwise Reduction of Graphene Oxide and Studies on Defect-Controlled Physical Properties. *Sci. Rep.* **2024**, *14* (1), 294.
(86) Sookhakian, M.; Tong, G. B.; Alias, Y. In-Situ Electrodeposition of Rhodium Nanoparticles Anchored on Reduced Graphene Oxide Nanosheets as an Efficient Oxygen Reduction Electrocatalyst. *Appl. Organomet. Chem.* **2020**, *34*, No. e5370.

https://doi.org/10.1021/acsomega.4c05745
ACS Omega 2025, 10, 3338−3350